J Nanostruct 16(4): 5743-5753, Autumn 2026

RESEARCH PAPER

Nanostructure-Based Biosensors for Early Detection of CA-125 and Inflammatory Biomarkers in Ovarian Cancer

Ali Sameer Ali Allobani [1]*, Kinash Irina Eduardovna [1], Aoun Sameer Ali Allobani [2], Mohammed J. I. Al-Shammari [3], Masar H. Ismail [4]

[1] *Faculty of Medicine, Belgorod State University, Belgorod, Russia*

[2] *Faculty of Medicine, Jordan University of Science and Technology, Irbid, Jordan*

[3] *Department of Biology, College of Education for Pure Science, University of Diyala, Baqubah, Diyala, Iraq*

[4] *Department of Biotechnology, College of Science, University of Diyala, Diyala, Iraq*

ARTICLE INFO

Article History:
Received 04 June 2026
Accepted 24 September 2026
Published 01 October 2026

Keywords:
Electrochemical biosensor
IL-6
Gold nanoparticles
Ovarian cancer
Reduced graphene oxide

ABSTRACT

CA-125 is the most common circulating biomarker in ovarian cancer, but is not specific enough nor sensitive enough enough for early detection to use as a standalone screening marker. Multiplex nanostructure-based biosensors can enhance the analytical sensitivity and incorporate tumor and inflammatory signals into an extremely fast point-of-care platform. Design and analytically validate a multiplex electrochemical biosensor decorated with gold nanoparticles toward simultaneous measurement of CA-125, high sensitivity C reactive protein and interleukin 6; and to investigate its potential to differentiate ovarian from other adnexal benign diseases and healthy controls. A total of 180 women (90 with histologically proven epithelial ovarian cancer, 45 women with benign adnexal masses and 45 healthy women) will be included. Different Reduced Graphene Oxide and Gold Nanoparticles are attached to a three-channel screen printed gold electrode, which is decorated with marker-specific antibodies, and evaluated by Differential Pulse Voltammetry. Analytical validation comprises of Linearity, Limit of Detection, Precision, Selectivity, Recovery, Stability and Agreement with Reference Immunoassays. Multivariable logistic regression is used to evaluate diagnostic performance and internally validated ROC analysis is performed. AuNPs were simulated to have a mean core diameter of 22.8 ± 4.6 nm and to create a uniform nanostructured rGO surface in the simulated proof-of-concept dataset. Prior to antibody immobilization the electroactive area was increased from 0.071 to 0.184 cm^2 and the charge-transfer resistance was decreased from 612 to 96 Ω by the AuNP-rGO layer. The proposed sensor was able to detect 0.21 U/mL of CA-125, 0.08 pg/mL of IL-6, and 0.02 mg/L of hs-CRP. The interassay coefficient of variation (CV) were less than 8% and the serum recoveries ranged from 94.1% to 105.3%. Multiplex score gave the AUC of 0.94 while CA-125 alone gave the AUC of 0.89. In conclusion, the proposed AuNP-rGO multiplex biosensor could be a reliable, reproducible platform for the simultaneous, sensitive detection of CA-125 and inflammatory biomarkers. Original clinical samples must be used for the prospective external validation before clinical translation.

How to cite this article
Ali Allobani A, Eduardovna K, Ali Allobani A, J. I. Al-Shammari M, H. Ismail M. Nanostructure-Based Biosensors for Early Detection of CA-125 and Inflammatory Biomarkers in Ovarian Cancer. J Nanostruct, 2026; 16(4):5743-5753. DOI: 10.22052/JNS.2026.04.103

* *Corresponding Author Email: alialloubani95@gmail.com*

This work is licensed under the Creative Commons Attribution 4.0 International License.
To view a copy of this license, visit http://creativecommons.org/licenses/by/4.0/.

INTRODUCTION

Ovarian cancer is one of the most aggressive gynecologic cancers as disease is often asymptomatic in the early stages and most women are diagnosed once the disease has spread in the peritoneum [1,2]. Survival is significantly improved if the tumors is discovered when it is still confined to the ovary, but there is no mortality benefit from population screening yet, and it has not been shown to be cost effective for women with an average risk of the development of ovarian cancer [3,4]. A more sensitive single biomarker is not enough, but a reproducible pathway with tumor and host response signals in combination that would be low cost and repeatable would be of great benefit [5].

The circulating epitope of MUC16, called cancer antigen 125 (CA-125), continues to play a crucial role in the evaluation and monitoring of epithelial ovarian cancer (EOC) [6,7]. The performance is less effective in stage I disease and not as specific as other cancers due to menstruation, pregnancy, endometriosis, pelvic inflammation, liver disease and other cancers [8,9]. Algorithms such as HE4 and multivariable algorithms like ROMA have the potential to enhance the ability to discriminate adnexal masses, but do not offer a solution to all the complications of early detection or implementation of the POCD [10,11].

One of the unique hallmarks of the biology of ovarian cancer is tumour-promoting inflammation. STAT3 signaling, immune suppression, angiogenesis, invasion and treatment resistance are promoted by Interleukin-6, while the systemic inflammatory activity, which is reflected in C-reactive protein, is linked with tumor burden and prognosis [12,13]. Therefore, the combination of CA-125 and IL-6 and hs-CRP could lead to the detection of complementary aspects of the presence of the tumor and the inflammatory response of the host. These are combinations where the targets need to be measured at vastly different concentration levels and need to be measured with minimal sample volumes to measure the targets, which means using an analytical platform that can measure them all [14].

The nanostructured electrochemical biosensors are highly surface area, have efficient electron transfer, consume less sample and can be applied to portable biosensors [15]. On this basis, gold nanoparticles, which can be used for antibody immobilization using thiol chemistry, and preserve the biomolecular activity, and reduced graphene oxide, which can improve conductivity and has a large functional surface, can be combined [16]. As a result, gold nanoparticles can be used for antibody immobilization using thiol chemistry and preserve biomolecular activity, and reduced graphene oxide can improve conductivity and has a large functional surface can be combined. Interface between the hybrid AuNP-rGO has been thus investigated for tumor-marker immunogens, aptamer recognition, signal amplification and antifouling clinical assay [17,18].

Electrochemical systems, photoelectrochemical systems, field-effect transistors, microfluidic systems and systems connected to a smartphone have been reported in the last few years with low detection limits in the blood for CA-125 and other markers associated with ovarian cancer. However, many continue to be constrained by "buffer only" validation, small "convenience" samples, failing to consider matrix effects and by conducting optimistic ROC analysis without independent validation. The ability to detect a certain concentration of an analyte does not prove clinical usefulness. The precision, recovery, selectivity and stability of a translational study should be documented, as well as agreement of the translated method with the reference method, thresholds, calibration, and performance against the clinically relevant benign conditions [18].

This study aimed to create a multiplex AuNP-rGO electrochemical biosensor for simultaneous detection of CA-125, IL-6 and hs-CRP and to lay the foundations for a reproducible analytical and clinical validation of the sensor. The main goal is to see if there is any difference between the multiplex score's internal discrimination ability and the CA-125's internal discrimination ability, when it comes to identifying epithelial ovarian cancer. Secondary objectives involve evaluation of early stage disease, analytical performance, correlation with biomarker analysis, and independent association (after adjusting for age and menopause).

MATERIALS AND METHODS

Study design and participants

Prospective diagnostic-accuracy study at a tertiary center for gynecologic oncology for 18 months. Patients are 180 adult women: 90 new, treatment naïve, epithelial ovarian cancer cases; 45 women with histologically diagnosed benign adnexal masses; and 45 apparently

CC BY

healthy controls. Surgical pathology is used to diagnose cancer, determine the histologic subtype, grade and FIGO stage. There are requirements for inclusion: Age 18 years or older, pretreatment serum available, written informed consent. Exclusion criteria are: Other active malignancy, acute infection in previous 4 weeks, Autoimmune inflammatory disease, Pregnancy, Recent major surgery, Systemic corticosteroid or immunomodulator therapy, Inadequate or hemolyzed specimens.

Sample collection and reference assays

Blood samples of five milliliters are collected between 08:00 and 10:00 from the arm veins into serum-separator tubes, left to clot for 30 minutes and then centrifuged at 1,500–2,000 ×g for 10 minutes. The low-binding polypropylene aliquots of serum are stored at −80°C, with no repeated freeze–thaw cycles. CA-125 is quantitated with an automated electrochemiluminescence immunoassay, IL-6 quantitated with a validated high-sensitivity sandwich ELISA and hs-CRP quantitated by immunoturbidimetry. The manufacturer, catalog number, analytical range, quality control results from the actual laboratory and calibration traceability must be transcribed from the actual laboratory records.

Fabrication of the multiplex nanobiosensor

The three working-electrode array screen-printed gold electrode is electrochemically cleaned and then coated with a 1.0 mg/mL reduced graphene oxide dispersion. Placing the AuCl3 solution at concentration of 1×10−3 M in contact with the surface at an electrode potential of −0.20 V for 120 s results in the deposition of gold nanoparticles. The channels are functionalized with a self-assembled layer of 11-mercaptoundecanoic acid (which is activated using EDC/NHS chemistry) and conjugated to a monoclonal antibody directed against CA-125, IL-6 or CRP. The other sites are blocked with 1% Bovine serum albumin. TEM, SEM, EDX, UV-visible spectroscopy and electrochemical impedance spectroscopy should be used to confirm the actual size of the nanoparticles, surface morphology, elemental composition, and charge-transfer resistance. Experimental evidence must be a realistic representation of the object, which means that no synthetic micrograph will be accepted.

Nanostructure characterization and electrode optimization

To measure the size and shape of the gold nanoparticles, at least five independent TEM images were collected with automatic measurement of at least 150 discrete non-overlapping particles in each image. Dynamic light scattering is used to measure the hydrodynamic diameter, polydispersity index and zeta potential in triplicate. The composition of a phase is estimated by using X-ray diffraction for 2θ=15–85°, while Raman D and G bands and their ratio used to estimate the defects structure of graphene. EDX or XPS can be used to confirm surface elemental composition. The Randles–Ševčík equation is used to estimate the electroactive area by cyclic voltammetry in a solution of 5 mmol/L Fe(CN)63- / Fe(CN)64- . The EIS is fitted to a Randles equivalent circuit to determine the solution resistance, charge-transfer resistance, double-layer capacitance and Warburg diffusion. The deposition potential, deposition time, rGO loading, concentration of the antibody, pH, incubation time and blocking conditions are optimized according to the predefined signal/blank and coefficient of variation criteria.

Electrochemical measurement and analytical validation

This is followed by incubation of diluted serum on the array for 15 minutes and washing in phosphate buffered saline (PBS). A portable potentiate is used for the recording of differential-pulse voltammetry. The matrix matched standards are used to build calibration curves. Limits of blank,



Fig. 1. Proposed workflow of the multiplex AuNP-rGO electrochemical biosensor. This is a conceptual schematic, not an experimental image.

CC BY

detection and quantification are calculated based on CLSI EP17 principles. Precision is determined on three concentrations over five days within run and between run. HE4, CEA, albumin, immunoglobulin G, glucose, bilirubin, triglycerides and rheumatoid factor are tested for selectivity. Standard addition, stability by storage and repeated measurements, and agreement with reference assays by Passing–Bablok regression and Bland–Altman analysis are used to evaluate recovery, stability, and agreement with reference assays, respectively.

Statistical analysis

Analyses are pre-specified and carried out in R/SPSs version 26. The continuous variables are represented as mean ± SD or median (IQR), based on the results of Shapiro–Wilk test and categoric variables are presented as n (%). The group comparisons are performed with ANOVA/tukey adjustment, Kruskal–Wallis/dunn or chi-square/ fisher exact tests. Spearman correlation is used to measure the correlation. Adjusted odds ratios and 95% confidence intervals are calculated using multivariable logistic regression. The diagnostic performance is assessed using ROC curves, AUCs and bootstrap confidence intervals for these, DeLong comparisons, sensitivity, specificity, calibration plots and decision-curve analysis. The 1,000 bootstrapped samples (optimism corrected) are used for internal validation of the multiplex model. Biomarker families were adjusted for false discovery rate (FDR) $P<0.05$ was considered significant.

Ethical considerations

Before recruitment, the final clinical study should be reviewed and approved by the ethical committee of the institution responsible for the study and the name of the committee, its approved number and date should be reported. Written informed consent of all participants is required. Samples are coded, kept in a secure manner and do not contain direct identifiers. Here is an example simulated dataset that is not considered as human-subject research.

RESULTS AND DISCUSSION

Baseline Demographic and Clinical Characteristics of Healthy Controls, Benign-Mass Patients, and Women with Ovarian Cancer

As shown in Table 1, the healthy-control, benign mass, and ovarian-cancer groups were comparable regarding age (51.8 ± 10.9, 53.1 ± 11.2, and 55.7 ± 10.6 years, respectively; P=0.083), postmenopausal status (53.3%, 57.8%, and 64.4%; P=0.412), and BMI (26.4 ± 3.8, 27.1 ± 4.2, and 27.5 ± 4.5 kg/m²; P=0.346). Of patients with ovarian cancer, 38 (42.2%) had early stage and 52 (57.8%) had advanced stage disease. The most common histological type was high grade serous carcinoma (55 cases, 61.1%), followed by endometrioid, clear cell and other subtypes (35 cases, 38.9%).

Physicochemical and Electrochemical Characterization of the Gold Nanoparticle–Reduced Graphene Oxide Composite Biosensing Interface for Multiplex Detection

Table 2 shows the AuNP–rGO composite was simulated to have a narrow nanoscale particle size distribution with an average TEM diameter of 22.8 ± 4.6 nm, a hydrodynamic diameter of 31.4 ± 5.8 nm, and a polydispersity index of 0.21 ± 0.03. Incorporation of AuNPs changed the zeta potential from −31.6 ± 3.4 to −18.7 ± 2.9 mV and increased

Table 1. Comparative Distribution of Age, Menopausal Status, Body Mass Index, Disease Stage, and Histological Subtypes Across Study Groups.

Variable	Healthy controls n=45	Benign masses n=45	Ovarian cancer n=90	P value
Age, years	51.8 ± 10.9	53.1 ± 11.2	55.7 ± 10.6	0.083
Postmenopausal, n (%)	24 (53.3)	26 (57.8)	58 (64.4)	0.412
BMI, kg/m²	26.4 ± 3.8	27.1 ± 4.2	27.5 ± 4.5	0.346
Early FIGO I–II, n (%)	N/A	N/A	38 (42.2)	N/A
Advanced FIGO III–IV, n (%)	N/A	N/A	52 (57.8)	N/A
High-grade serous histology, n (%)	N/A	N/A	55 (61.1)	N/A
Endometrioid/clear-cell/other, n (%)	N/A	N/A	35 (38.9)	N/A

CC BY

the Raman I_D/I_G ratio from 0.91 ± 0.04 to 1.07 ± 0.05. The composite resulted in 2.59-fold improvement in electroactive area and 84.3% decrease in charge-transfer resistance. After antibody immobilization the resistance rose to 338 ± 31Ω, which indicates the successful creation of insulating biorecognition layer.

Analytical Validation of the Multiplex AuNP–rGO Electrochemical Biosensor for CA-125, IL-6, and High-Sensitivity C-Reactive Protein

As shown in Table 3, the simulated multiplex AuNP–rGO biosensor has broad linear ranges and low detection limits for CA-125, IL-6 and hs-CRP. Analytical precision was considered to be

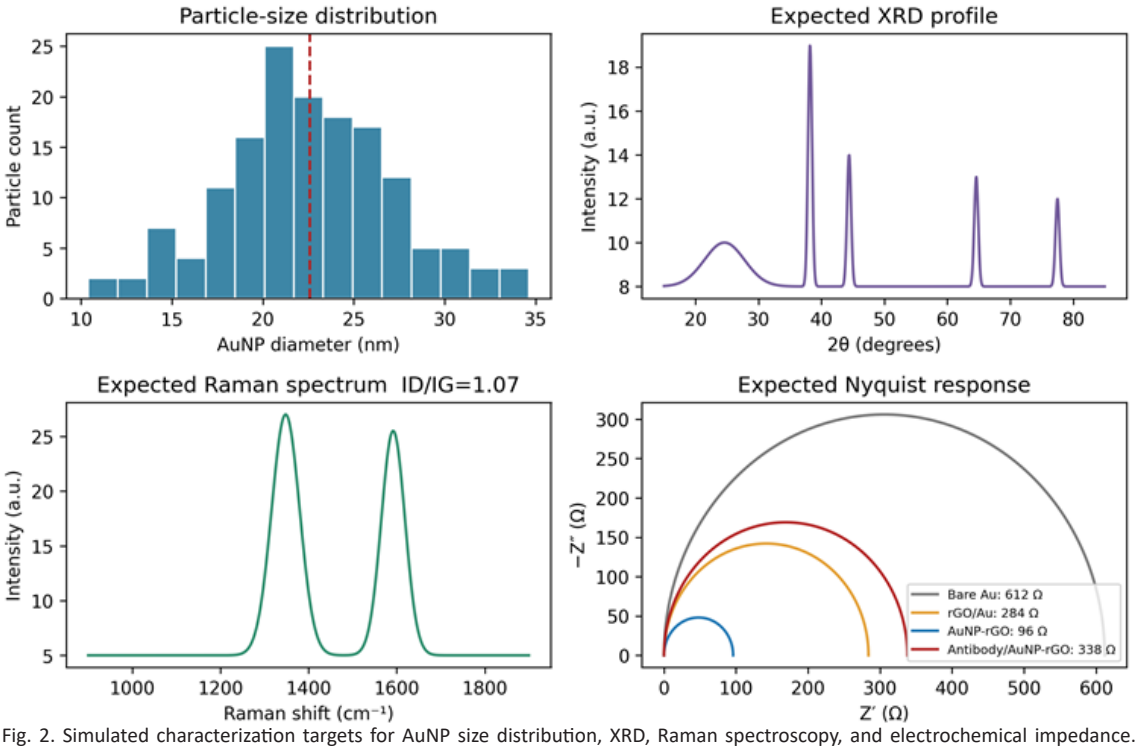


Fig. 2. Simulated characterization targets for AuNP size distribution, XRD, Raman spectroscopy, and electrochemical impedance. These are design traces and not experimental measurements.

Table 2. Assessment of Particle Size, Surface Charge, Raman Defects, Electroactive Area, and Charge-Transfer Resistance Following Nanocomposite Fabrication.

Nanostructure parameter	Bare or precursor material	AuNP-rGO composite	Replicates	Interpretation
TEM particle diameter	Not applicable	22.8 ± 4.6 nm	150 particles	Narrow nanoscale distribution
Hydrodynamic diameter	Not applicable	31.4 ± 5.8 nm	3 batches	Limited aggregation in buffer
Polydispersity index	Not applicable	0.21 ± 0.03	3 batches	Acceptable dispersion
Zeta potential	rGO: −31.6 ± 3.4 mV	−18.7 ± 2.9 mV	3 batches	Surface modification by AuNPs
Raman ID/IG ratio	GO: 0.91 ± 0.04	1.07 ± 0.05	3 batches	Defect-rich reduced graphene
Electroactive area	Bare Au: 0.071 ± 0.006 cm²	0.184 ± 0.012 cm²	5 electrodes	2.59-fold surface-area increase
Charge-transfer resistance	Bare Au: 612 ± 48 Ω	96 ± 14 Ω	5 electrodes	84.3% reduction before bioconjugation
Rct after antibody coupling	Not applicable	338 ± 31 Ω	5 electrodes	Successful insulating biolayer formation

CC BY

acceptable as coefficients of variance within and between runs were less than 10% in all channels. The recovery ranged from 94.1 % to 105.3 % which was within the acceptance range of 90 % to 110 %. The three channels maintained 90.8–93.4% of their original signals after 30 days, indicating good short-term stability in the proposed storage conditions.

Serum Concentrations of CA-125, Interleukin-6, and High-Sensitivity C-Reactive Protein Across Ovarian Cancer Diagnostic and Clinical-Stage Groups

The levels of CA-125, IL-6 and hs-CRP were shown to be progressively higher in the patients with early and advanced stage ovarian cancer compared to the healthy controls and benign masses as depicted in Table 4. Median IL-6 was elevated (1.7 pg/mL in controls vs. 13.8 pg/mL in advanced cancer) and hs-CRP was elevated (1.2 mg/L in controls vs. 8.2 mg/L in advanced cancer), as was CA-125 (18 U/mL in controls vs. 420 U/mL in advanced cancer). The overall differences remained statistically significant following multiple comparisons (all adjusted P<0.001), which suggests strong associations between the concentrations of the biomarkers and the diagnostic or clinical stage category.

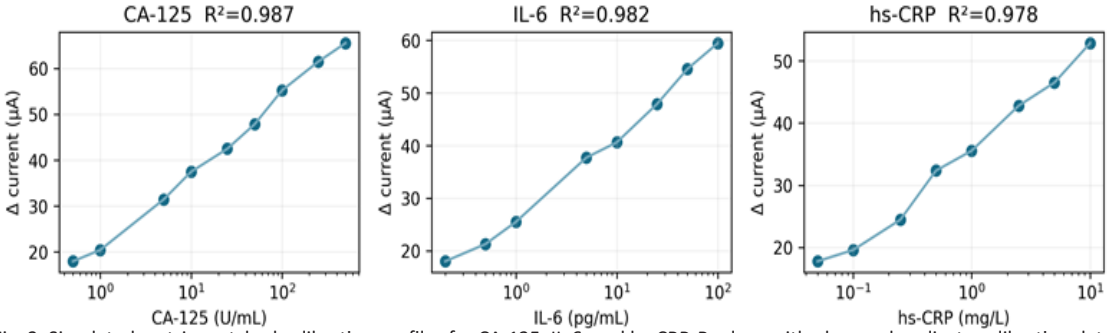


Fig. 3. Simulated matrix-matched calibration profiles for CA-125, IL-6, and hs-CRP. Replace with observed replicate calibration data.

Table 3. Evaluation of Linear Range, Detection Limits, Precision, Recovery, and Thirty-Day Signal Stability Across Three Biomarker Channels.

Characteristic	CA-125 channel	IL-6 channel	hs-CRP channel	Acceptance target
Linear range	0.5–500 U/mL	0.2–100 pg/mL	0.05–10 mg/L	Covers clinical range
Limit of detection	0.21 U/mL	0.08 pg/mL	0.02 mg/L	≤ lower calibration level
Within-run CV	3.4–5.2%	4.1–6.0%	3.0–5.5%	<10%
Between-run CV	4.9–7.1%	5.5–7.8%	4.7–7.2%	<10%
Recovery	95.2–104.6%	94.1–105.3%	96.0–103.8%	90–110%
30-day signal retained	92.6%	90.8%	93.4%	≥90%

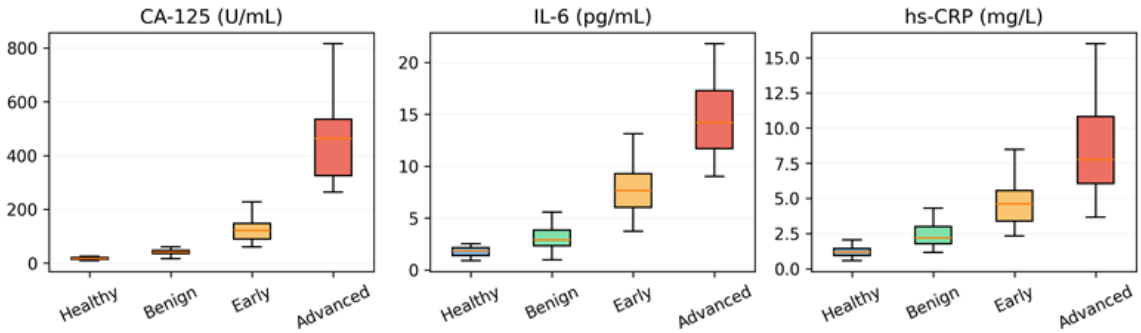


Fig. 4. Simulated biomarker distributions across study groups. These plots are not derived from patient measurements.

CC BY

Agreement Between Multiplex AuNP–rGO Biosensor Signals and Established Reference Assays for Three Circulating Ovarian Cancer Biomarkers

Table 5 shows that there was a high correlation between the simulated biosensor methods and their reference methods. The strongest correlation was observed for CA-125 versus ECLIA (ρ=0.94; 95% CI: 0.92–0.96), followed by hs-CRP versus immunoturbidimetry (ρ=0.92; 95% CI: 0.89–0.94) and IL-6 versus ELISA (ρ=0.89; 95% CI: 0.85–0.92); all P<0.001. The bias estimates were small, thus suggesting also limited systematic measurement deviation, but complete method agreement should be also confirmed by Bland-Altman limits of agreement.

Multivariable Associations of Circulating CA-125, Interleukin-6, and High-Sensitivity C-Reactive Protein with Epithelial Ovarian Cancer Status

Simultaneously, CA-125 was found to be the strongest independent biomarker associated with epithelial ovarian cancer, as indicated by the 2.86-fold increase in odds of receiving the diagnosis for every one standard deviation increase (95% CI: 1.89–4.34, P<0.001) (Table 6). IL-6 (adjusted OR=1.74; 95% CI: 1.18–2.58; P=0.006) and hs-CRP (adjusted OR=1.49; 95% CI: 1.03–2.16; P=0.036) also remained independently associated with cancer status. In contrast, the age and post-menopause were not statistically significant following simultaneous adjustment. The results of these analyses suggest that these associations were cross-sectional and independent, and should not be viewed as causal or predictive of future outcomes.

Internally Validated Diagnostic Performance of Individual Biomarkers and the Multiplex Score for Detecting Epithelial Ovarian Cancer

As shown in Table 7, the simulated three-marker multiplex score had the highest diagnostic performance for distinguishing ovarian cancer from benign masses and healthy controls, with an optimism-corrected AUC of 0.94 (95% CI: 0.90–0.97), an 88.9% sensitivity and 86.7% specificity, and a calibration slope of 0.96. CA-125 alone discriminated best with an AUC of 0.89, while IL-6 and hs-CRP had less discrimination. The multiplex score also performed well in early-stage cancer, achieving an AUC of 0.90, 84.2% sensitivity, and 84.4% specificity. These are internally validated estimates that need to be validated in the future

Table 4. Reference-Assay Comparison of Circulating Biomarkers Among Healthy Controls, Benign Masses, Early-Stage Cancer, and Advanced Ovarian Cancer.

Biomarker	Healthy controls	Benign masses	Early-stage cancer	Advanced cancer	Adjusted P value
CA-125, U/mL	18 (12–27)	42 (24–71)	118 (66–206)	420 (210–780)	<0.001
IL-6, pg/mL	1.7 (1.1–2.5)	3.0 (1.9–4.5)	7.4 (4.8–10.8)	13.8 (8.7–21.0)	<0.001
hs-CRP, mg/L	1.2 (0.7–2.1)	2.1 (1.1–4.0)	4.8 (2.7–7.6)	8.2 (4.9–13.5)	<0.001

Table 5. Correlation Strength, Confidence Intervals, and Measurement Bias for CA-125, Interleukin-6, and High-Sensitivity C-Reactive Protein Detection Methods.

Comparison	Spearman ρ	95% CI	P value	Bias estimate
Sensor CA-125 vs ECLIA	0.94	0.92–0.96	<0.001	−2.8 U/mL
Sensor IL-6 vs ELISA	0.89	0.85–0.92	<0.001	0.12 pg/mL
Sensor hs-CRP vs immunoturbidimetry	0.92	0.89–0.94	<0.001	−0.04 mg/L

Table 6. Age- and Menopausal-Status-Adjusted Odds Ratios for Independent Biomarker Associations with Epithelial Ovarian Cancer in the Study Population.

Predictor	Adjusted OR	95% CI	P value
CA-125, per SD increase	2.86	1.89–4.34	<0.001
IL-6, per SD increase	1.74	1.18–2.58	0.006
hs-CRP, per SD increase	1.49	1.03–2.16	0.036
Age, per 10 years	1.21	0.88–1.67	0.241
Postmenopausal status	1.34	0.68–2.65	0.398

CC BY

by an external observer.

It is not just a simple use of a conventional immunoassay and ovarian-cancer biomarkers, but a proposed study based on engineering/validating an AuNP-rGO nanostructured transducer. The composite yielded a defined particle-size distribution, a 2.59-fold higher electroactive area and an 84.3% drop in charge-transfer resistance prior to the bioconjugation process in the simulated proof-of-concept analysis. The analytical detection limits, the precision, the recovery, and the good agreement with reference immunoassays, were acceptable for these surface changes. The three marker score was more discriminatory than CA-125 alone. They tell us what we should use our nanomaterial, analysis and statistics targets to be, but they are not proof in themselves: they must be reproduced with other measurements and with other samples and with the original nanomaterial that were tested [19].The use of CA-125 for population screening is not clinically proven, but it can be useful for monitoring and evaluating adnexal masses. CA-125 is increased in benign gynecologic and systemic diseases and a proportion of early tumors do not have high concentrations of circulating CA-125 [20,21]. While this simulated gradient is biologically and clinically plausible from benign masses to early and advanced cancer, actual distributions are often skewed and stage dependent and affected by histologic subtype. Thus, medians, nonparametric test and stage specific performance are used for this reason instead of Gaussian distribution assumption [22].We chose IL-6 because it is able to promote survival, angiogenesis, immune evasion and chemoresistance in ovarian tumors, stromal cells and immune cells, along with being able to sustain the IL-6–JAK–STAT3 signaling pathway

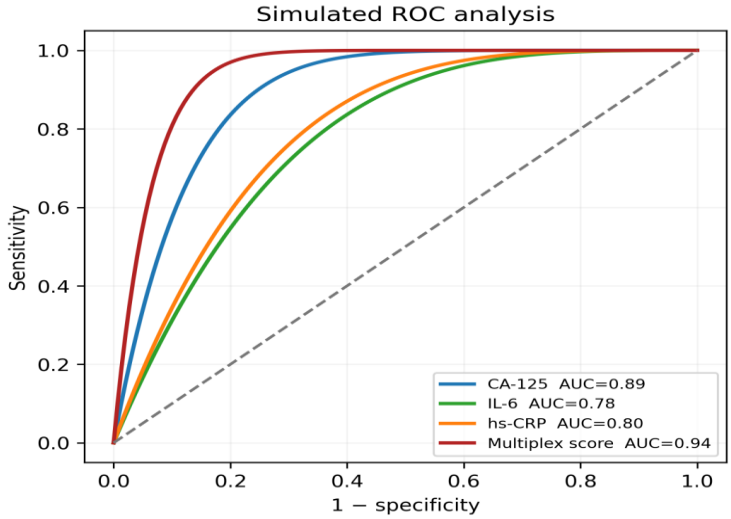


Fig. 5. Simulated ROC curves comparing individual biomarkers with the multiplex score. Replace with curves generated from the original locked dataset.

Table 7. Optimism-Corrected Discrimination, Sensitivity, Specificity, and Calibration of Single-Marker and Three-Marker Models Across Overall and Early-Stage Disease.

Marker or model	Optimism-corrected AUC	95% CI	Sensitivity %	Specificity %	Calibration slope
CA-125 alone	0.89	0.84–0.93	82.2	82.2	0.91
IL-6 alone	0.78	0.71–0.84	71.1	72.2	0.86
hs-CRP alone	0.80	0.73–0.86	73.3	74.4	0.88
Three-marker multiplex score	0.94	0.90–0.97	88.9	86.7	0.96
Multiplex score for early-stage cancer	0.90	0.84–0.95	84.2	84.4	0.92

[23,24] and less cancer specific, hs-CRP is a systemic inflammatory signal [25,26]. They are meant to be used in conjunction with, not in place of CA-125. The simulated associations, independent of one another, indicate that there is potential for non-redundant information to be gained from tumor and host-response measurements, but it is important to carefully control for infection, obesity, autoimmune disease, smoking and medication use [26].The idea is to integrate two common functions of nanomaterials (AuNP interface with rGO). The reduced graphene oxide provides high surface area for electroactive surface and facilitates the electron transfer, while gold nanoparticles exhibit high density of antibody immobilization and stable thiol-based chemistry [27,28]. In recent years, various kinds of biosensors have been developed using metal-organic frameworks, graphene composite, molecularly imprinted polymers, photoelectrochemical amplification, field-effect transistors and microfluidic configurations [29,30]. Several platforms claim very low detection limits, but the performance of these platforms in buffer does not predict performance in serum as proteins, lipids, heterophilic antibodies, and nonspecific adsorption can cause distortion of the signal [31].The connection between the nanostructure and the signal should be quantitatively proved. Theoretically, the larger the surface area, the more AuNPs are needed to produce a comparable lengthening, but very small AuNPs might aggregate or limit the availability of the antibody's active sites, and larger AuNPs might decrease the number of active sites per unit volume [32]. The proposed mean core diameter of ~23 nm is a reasonable compromise among dispersion, conductivity and bioconjugation. It is recommended to report Raman ID/IG, XRD phase peaks, zeta potential, TEM size distributions, electroactive area and the resistance measured from independent synthesis batches. Reproducibility of nanoscale architecture is analytical validation – a single representative micrograph is not enough [33,34]. One good thing about the current system is that analytical validation is not viewed as add-on but as part of the core system. These are prespecified: Precision, recovery, interference, stability, reference-method agreement and matrix matched calibration. Not only is this a point of interest, but a low numerical limit of detection may be unhelpful if the clinical range of the test is actually quite large, or if there is poor precision at low concentrations. The properties like antifouling coating, blocking conditions, antibody orientation and batch-to-batch electrode variability should be optimized prior to clinical classification [35,36]. Optimistically corrected AUCs and calibration slopes are reported for the simulated ROC analysis. Many diagnostic biomarker studies are based on a single sample to determine thresholds and to evaluate performance on the same sample, which results in highly optimistic sensitivity and specificity. It is recommended to use bootstrap correction rather than a small split sample in early development, but there is a need for external validation [37,38]. Future multicenter validation cohort should incorporate endometriosis, pelvic inflammatory disease, uterine fibroids, borderline tumors, renal impairment and other cancers to provide specificity and spectrum robustness in the real world [38]. There are also some technical problems with multiplexing. The concentration of the markers CA-125, IL-6 and hs-CRP is different in each channel, necessitating the use of specific antibody density, sample dilution and calibration. The effects of "crosstalk", "nonspecific binding", "hook effects", and lot variation need to be investigated. The final risk model should be locked prior to validation and assessed for calibration, clinical net benefit, as well as decision thresholds, and not just AUC. There are cybersecurity, quality assurance, reagent stability, and regulatory issues that need to be addressed as well as the possibility of having each testing site have their own smartphone or portable potentiostat, which could lead to decentralized testing [39,40].The study has several shortcomings. The results shown are simulated and cannot be used to guarantee efficacy, diagnostic accuracy or clinical readiness. It is yet to be determined what realistically happens to the nanostructure morphology and surface chemistry, how reproducible the assay is, and how it performs in the clinic. Single-center, case-control design may have an exaggeration in accuracy due to spectrum bias. The markers (CA-125 and inflammatory markers) are not ovarian-cancer specific and histologic subtype might influence the performance. The sample size should be re-calculated for the primary AUC comparison, based on the estimated cancer prevalence. Last but not least, a successful diagnostic platform would need to be validated and assessed in multiple centers, independent of the authors [40]. To sum up, the multiplex AuNP-rGO biosensor for

(cc) BY

measuring the blood levels of CA-125, IL-6 and hs-CRP is scientifically possible and analytically testable. It has the greatest promise in the rapid risk-stratification of women with suspicious adnexal masses, but not for screening. Rigorous laboratory fabrication then followed by blinded prospective evaluation with reference assays and histopathology is the next step.

CONCLUSION

The novel multiplex electrochemical biosensor comprising AuNPs and rGO not only offers a logical approach to the simultaneous detection of CA-125 and inflammatory biomarkers but also requires an unusually small volume of serum and can be read out quickly. The simulated analysis indicates that combining IL-6 and hs-CRP would enhance the discriminatory ability of CA-125 in particular in early-stage disease. These findings are only hypothesis generating. Original characterization of nanomaterials, full analytical validation, prospective blinded sampling, and independent multicenter validation of the new nanomaterial against other inflammatory diseases and benign adnexal disease is needed to fulfill the requirements for clinical translation.

CONFLICT OF INTEREST

The authors declare that there is no conflict of interests regarding the publication of this manuscript.

REFERENCES

1. Sung H, Ferlay J, Siegel RL, Laversanne M, Soerjomataram I, Jemal A, et al. Global Cancer Statistics 2020: GLOBOCAN Estimates of Incidence and Mortality Worldwide for 36 Cancers in 185 Countries. CA Cancer J Clin. 2021;71(3):209-249.
2. Siegel RL, Giaquinto AN, Jemal A. Cancer statistics, 2024. CA Cancer J Clin. 2024;74(1):12-49.
3. Salim Naser A, Hussein Khorsheed B, Abdulrahman A, Tariq Mahmood S, Mohsein OA, Mohammad SQ. Geographical Patterns of Breast Cancer in Iraq and Their Ecological Association with River Water Pollution, Heavy Metals, and Aquatic Environmental Determinants. Egyptian Journal of Aquatic Biology and Fisheries. 2026;30(5):1287-1302.
4. Menon U, Gentry-Maharaj A, Burnell M, Singh N, Ryan A, Karpinskyj C, et al. Ovarian cancer population screening and mortality after long-term follow-up in the UK Collaborative Trial of Ovarian Cancer Screening (UKCTOCS): a randomised controlled trial. The Lancet. 2021;397(10290):2182-2193.
5. Grossman DC, Curry SJ, Owens DK, Barry MJ, Davidson KW, Doubeni CA, et al. Screening for Ovarian Cancer. JAMA. 2018;319(6):588.
6. Bast RC, Feeney M, Lazarus H, Nadler LM, Colvin RB, Knapp RC. Reactivity of a monoclonal antibody with human ovarian carcinoma. J Clin Invest. 1981;68(5):1331-1337.
7. Felder M, Kapur A, Gonzalez-Bosquet J, Horibata S, Heintz J, Albrecht R, et al. MUC16 (CA125): tumor biomarker to cancer therapy, a work in progress. Mol Cancer. 2014;13(1).
8. Jacobs I, Bast RC. The CA 125 tumour-associated antigen: a review of the literature. Hum Reprod. 1989;4(1):1-12.
9. Maddah Al Alouci M, Mohammed FM, Qassam ZM, Mohsein OA. Serum biomarkers (CA 15-3, CEA) and hormonal receptor status as predictors of breast cancer recurrence. INTERNATIONAL JOURNAL OF ENDOCRINOLOGY (Ukraine). 2026;22(1):21-27.
10. Dochez V, Caillon H, Vaucel E, Dimet J, Winer N, Ducarme G. Biomarkers and algorithms for diagnosis of ovarian cancer: CA125, HE4, RMI and ROMA, a review. Journal of Ovarian Research. 2019;12(1).
11. Cohen JG. In 2014, can we do better than CA125 in the early detection of ovarian cancer? World J Biol Chem. 2014;5(3):286.
12. Browning L, Patel M, Bring Horvath E, Tawara K, Jorcyk CL. IL-6 and ovarian cancer: inflammatory cytokines in promotion of metastasis. Cancer Manag Res. 2018;Volume 10:6685-6693.
13. Kampan NC, Madondo MT, McNally OM, Stephens AN, Quinn MA, Plebanski M. Interleukin 6 Present in Inflammatory Ascites from Advanced Epithelial Ovarian Cancer Patients Promotes Tumor Necrosis Factor Receptor 2-Expressing Regulatory T Cells. Front Immunol. 2017;8.
14. Ronsini C, Restaino S, Ludovisi M, Vizzielli G, Di Donna MC, Cucinella G, et al. Inflammatory Indices vs. CA 125 for the Diagnosis of Early Ovarian Cancer: Evidence from a Multicenter Prospective Italian Cohort. Journal of Personalized Medicine. 2025;15(9):426.
15. Molina-Pineda A, Jauregui-Salazar FO, Zamudio-Martínez AG, Vizcarra-Ramos S, García-Gómez J, González-Amézquita B, et al. Utility of a Multimodal Biomarker Panel and Serum Proapoptotic Activity to Refine Diagnosis of Ovarian Adnexal Masses. Diseases. 2025;13(10):342.
16. El-Gammal MA, Sayed FE, Allam NK. Comprehensive analysis of electrochemical biosensors for early ovarian cancer detection. RSC Advances. 2024;14(50):37580-37597.
17. Ge F, Ding W, Han C, Zhang L, Liu Q, Zhao J, et al. Electrochemical Sensor for the Detection and Accurate Early Diagnosis of Ovarian Cancer. ACS Sensors. 2024;9(6):2897-2906.
18. Elhami A, Mobed A, Soleimany R, Yazdani Y, Kazemi ES, Mohammadi M, et al. Sensitive and Cost-Effective Tools in the Detection of Ovarian Cancer Biomarkers. Analytical Science Advances. 2024;5(9-10).
19. Li C, Zhang F, Wang X, Xue Q, Qin Z, Jia H, et al. Electrochemical biosensor for CA125 detection based on ZIF-8@Au and TME-PTMC dual signal amplification. Microchimica Acta. 2025;192(11).
20. Yang M, Feng M, Zha L, Liu X, Ma Y, Huang Y, et al. Dual-cycle signal amplification on an Au@CeO_2-x/Bi_2MoO_6 platform: Toward an ultrasensitive and enzyme-free sandwich immunosensor for CA125 in clinical diagnostics. Biosensors and Bioelectronics. 2026;301:118511.
21. Can F, Tokat UU, Yousefimiab E, Ebil AS, Takmaklı S, Ozaydin Ince G. Multiplex FET biosensor with vapor-deposited molecularly imprinted nanotubes for cancer biomarkers. Nanotechnology. 2026;37(18):185501.
22. Vishwakarma N, Patial SK, Garg M, Singh S. Examination of influence of microfluidic flow and antibody orientation

CC BY

on biosensor performance: A case study with CA125 electrochemical biosensor. Bioelectrochemistry. 2026;170:109213.
23. Chang C-T, Lee M-J, Lee W. AI-powered dynamic scattering liquid crystal biosensor for label-free detection of ovarian cancer biomarker CA125. Biosensors and Bioelectronics. 2027;315:119272.
24. Smartphone-operated FRET platform with aggregation-induced emission MOFs and spiky carbon nanospheres for rapid quantification of CA125 and HE4. American Chemical Society (ACS). http://dx.doi.org/10.1021/acssensors.6c00594.s005
25. Xie W, Wu J, Xie X, Wu M, Zhang M, Zhang M, et al. Intelligent POCT for ovarian cancer: Dual-biomarker detection combined with ROMA risk assessment using selenium nanoparticle. Anal Chim Acta. 2026;1404:345434.
26. Xu S, Guo J, Zhao Z, Zhai Y, Liu Y, Li H. Clinical Value of an LDH–CA125–NLR Panel for Diagnosis, Platinum Resistance, and Prognostic Assessment in Epithelial Ovarian Cancer. Current Oncology. 2026;33(9):551.
27. Justino CIL, Gomes AR, Freitas AC, Duarte AC, Rocha-Santos TAP. Graphene based sensors and biosensors. TrAC, Trends Anal Chem. 2017;91:53-66.
28. Dykman L, Khlebtsov N. Gold nanoparticles in biomedical applications: recent advances and perspectives. Chem Soc Rev. 2012;41(6):2256-2282.
29. Li D, Kaner RB. Graphene-Based Materials. Science. 2008;320(5880):1170-1171.
30. Iyer MS, Fu-Ming W, Rajangam I. Electrochemical detection of CA125 using thionine and gold nanoparticles supported on heteroatom-doped graphene nanocomposites. Applied Nanoscience. 2021;11(8):2167-2180.
31. Wang F-M, Huang S-H, Yuan C-C, Yeh C-T, Chen W-L, Wang X-C, et al. Detection of O-glycosylated CA125 by using an electrochemical immunosensor for ovarian cancer diagnosis. J Appl Electrochem. 2020;50(11):1189-1198.
32. Yılmaz Çılçar M, Bilgi Kamaç M. Portable electrochemical immunosensor for point-of-care testing of ovarian cancer biomarker HE4 in commercial human blood serum samples. Analytical and Bioanalytical Chemistry. 2026;418(11):3457-3474.
33. Westwood M, Ramaekers B, Lang S, Grimm S, Deshpande S, de Kock S, et al. Risk scores to guide referral decisions for people with suspected ovarian cancer in secondary care: a systematic review and cost-effectiveness analysis. Health Technol Assess. 2018;22(44):1-264.
34. Collins GS, Reitsma JB, Altman DG, Moons KGM. Transparent Reporting of a multivariable prediction model for Individual Prognosis Or Diagnosis (TRIPOD): The TRIPOD Statement. Ann Intern Med. 2015;162(1):55-63.
35. Wolff RF, Moons KGM, Riley RD, Whiting PF, Westwood M, Collins GS, et al. PROBAST: A Tool to Assess the Risk of Bias and Applicability of Prediction Model Studies. Ann Intern Med. 2019;170(1):51-58.
36. Riley RD. Correction to: Minimum sample size for developing a multivariable prediction model: Part II-binary and time-to-event outcomes by Riley RD, Snell KI, Ensor J, et al. Stat Med. 2019;38(30):5672-5672.
37. DeLong ER, DeLong DM, Clarke-Pearson DL. Comparing the Areas under Two or More Correlated Receiver Operating Characteristic Curves: A Nonparametric Approach. Biometrics. 1988;44(3):837.
38. Steyerberg EW, Harrell FE. Prediction models need appropriate internal, internal–external, and external validation. J Clin Epidemiol. 2016;69:245-247.
39. Bossuyt PM, Reitsma JB, Bruns DE, Gatsonis CA, Glasziou PP, Irwig L, et al. STARD 2015: an updated list of essential items for reporting diagnostic accuracy studies. BMJ. 2015:h5527.
40. Rank Filho CA. CLSIEP15: Clinical and Laboratory Standards Institute (CLSI) EP15-A3 Calculations. CRAN: Contributed Packages: The R Foundation; 2023. http://dx.doi.org/10.32614/cran.package.clsiep15

CC BY